Research Article Vol. 28, No. 24 / 23 November 2020 / Optics Express 36122
Optics EXPRESS

Versatile objectives with NA = 0.55 and NA = 0.78 for cold-atom experiments

SHAOKANG LI,[1,2] GANG LI,[1,2,3] PENGFEI YANG,[1,2] ZHIHUI WANG,[1,2] PENGFEI ZHANG,[1,2] AND TIANCAI ZHANG[1,2,4]

[1] *State Key Laboratory of Quantum Optics and Quantum Optics Devices, and Institute of Opto-Electronics, Shanxi University, Taiyuan 030006, China*
[2] *Collaborative Innovation Center of Extreme Optics, Shanxi University, Taiyuan 030006, China*
[3] *gangli@sxu.edu.cn*
[4] *tczhang@sxu.edu.cn*

Abstract: We present two sets of versatile high-numerical-apeture objectives suitable for various cold-atom experiments. The objectives are assembled entirely by the commercial on-shelf singlets. The two objectives are initially optimized at working wavelength of 852 nm with a standard 5-mm silica optical flat window. They have numerical apertures of NA=0.55 and NA=0.78, working distances of 23 and 12.8 mm, diffraction-limited fields of view of 98 and 15 μm, and spatial resolutions of 0.94 and 0.67 μm, respectively. These performances are simulated by the ray-tracing software and experimentally confirmed by imaging line patterns and a point-like emitter on a resolution chart. The two objectives can be further reoptimized at any single wavelengths from ultraviolet to near infrared and for various optical flat window with different thickness by only tuning one of lens spacing. The two objectives provide convenient and flexible options to observe and address individual atoms in single atom arrays or optical lattices for various cold-atom experiments.

1. Introduction

The system of cold atoms has been recognized as important platform for the study of quantum simulation, quantum computation, and quantum information processing [1–8]. In all the experimental setups, one of the most essential components is the high numerical aperture (NA) objective to image and address individual atom in an atom trap array or optical lattices. The higher NA means higher resolution and higher collection efficiency.

In the experimental platforms with single Rydberg neutral atoms or single ions [4–6,9–12], the spacing between individual atoms are usually on several μm level, but the distance between the atoms and surface of the vacumm window are usually on tens of millimeter (mm) level. Therefore, long working distance (WD) are preferred more than the NA. The NA usually is below 0.55. Up to now, there are several designs [13–18] with commercial on-shelf $\Phi1''$- or $\Phi2''$-size singlets for this purpose. However, the highest NA can only reach 0.44 [14,18]. Here we present a new design of objective with NA=0.55 and WD=23 mm by $\Phi2''$-size singlets for addressing individual atom in atom arrays. It can also be used to image individual atom in optical lattices if optimized for the blue or ultraviolet light.

In the experimental platforms of quantum gases in optical lattices [1–3,19,20], the spacing between individual atoms are on sub-μm level, therefore much higher resolution is requested to *in situ* image the atom. The objectives usually have NA around 0.7 with the WD about several mm [1,19,20] in near infrared region. By using the solid immersion technique [21] the NA can be further enhanced to 0.87 [3] and 0.92 [22] at the cost that the WD is reduced to sub-mm level. The ojective with lower NA around 0.5 is also possible to observe individual atoms in lattices if the working wavelength is in blue or ultraviolet regions [18,23]. Here we provide another new design of objective to image individual atoms in optical lattices with WD over ten

#408945 https://doi.org/10.1364/OE.408945
Journal © 2020 Received 1 Sep 2020; revised 25 Oct 2020; accepted 28 Oct 2020; published 13 Nov 2020

millimeters (12.5 mm) while NA can still reach 0.78. This objective is also entirely assembled with commercial on-shelf Φ2″- and Φ1″-size singlets.

The two objectives are initially designed at the working wavelength of 852 nm with 5-mm-thick silica window. The designed diffraction-limited fields of view (FOVs) are 98 and 15 μm with spatial resolutions of 0.94 and 0.67 μm, respectively. The performances are simulated by the ray-tracing software and experimentally confirmed by imaging the line patterns and a point-like emitter on a resolution chart. In addition, these two objectives can be reoptimized at any single wavelengths from ultraviolet to near infrared and with various of optical flat window with different thickness by tuning only one of lens spacing. The two objectives provide convenient and flexible options to observe and address individual atoms in single atom arrays or optical lattices.

2. NA= 0.55 objective

Figure 1 shows the mechanical structure of the NA= 0.55 objective. Six commercial on-shelf singlets (LC1093, LB1199, LA1399, LE1015, LE 1418, and LE1076 from Thorlabs Inc.) with size Φ2″ are mounted in lens tube with five custom-made spacing rings. The objective is initially designed at 852 nm for cesium experiments, where a 5-mm thick optical vacuum window is taken into account. The plano-concave, double-convex, plano-convex, and positive Meniscus lenses are arranged in order to compensate the spherical aberration induced by each spherical singlet. Three positive Meniscus lenses are placed with the focal length changing from long to short, e.g. LE1015 (f = 200 mm), LE1418 (f = 150 mm), and LE1076 (f = 100 mm), to gradually increase the NA to 0.55. The spaces between each two singlets are optimized by the commercial ray-tracing software (Zemax) and the performances are also simulated. The optimized objective prescription is given by Table 1 and the Zemax file can be found in Code 1 [24].

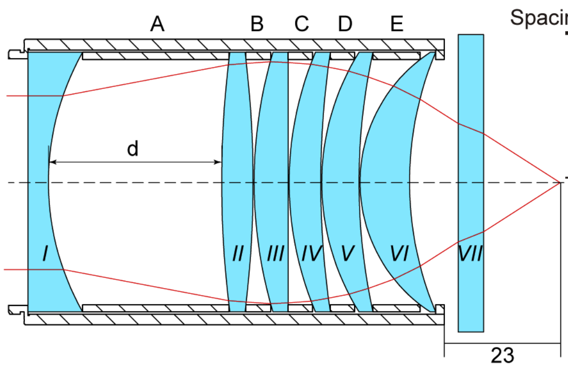

Spacing Rings	x (mm)
A	28.62
B	4.86
C	4.78
D	4.86
E	9.68

Fig. 1. Structure of the NA= 0.55 objective. The singlets marked with number *I*, *II*,. . . , and *VII* are LC1093, LB1199, LA1399, LE1015, LE 1418, LE1076, and optical flat. The material of the flat is silica and the thickness is 5 mm. The effective focal length of the objective is 30.95 mm at 852 nm.

Figure 2 displays the results of the simulation. The Strehl Ratio (SR) versus the point-like emitter displacement off the optical axis is shown in Fig. 2(a). The SR for the emitter on axis is 0.98, corresponding to a RMS (root mean square) wave front error of 2%λ, which means the objective corrects the aspheric aberration on axis almost perfectly. The diffraction-limited field of view (FOV) is defined as the region of displacement where the SR $\geq$ 0.8 [25]. The FOV for this objective is about 98 μm. The performances are further evaluated by simulating the modulation transfer function (MTF), as given by Fig. 2(b). Here, the simulated MTFs for point-like emitter on axis and 49 μm off the optical axis are compared with the ideal one. The results indicate that the imaging quality will be high enough at the edge of the FOV.

Optics EXPRESS

Table 1. The prescription of NA= 0.55 objective optimized at 852 nm and with 5-mm silica window (optical flat).

Surfce	Curvature (mm)	Thickness (mm)	Material	Part Number
1	∞	4	NBK7	LC1093
2	51.5	33.92 (d)	Air	
3	205	6.2	NBK7	LB1199
4	−205	0.2	Air	
5	90.1	6.7	NBK7	LA1399
6	∞	0.2	Air	
7	65.2	6.2	NBK7	LE1015
8	171.6	0.2	Air	
9	47.9	7.3	NBK7	LE 1418
10	119.3	0.2	Air	
11	30.3	9.7	NBK7	LE1076
12	65.8	9.47	Air	
13	∞	5 (T)	Silica	Optical Flat
14	∞	15	Vacuum	

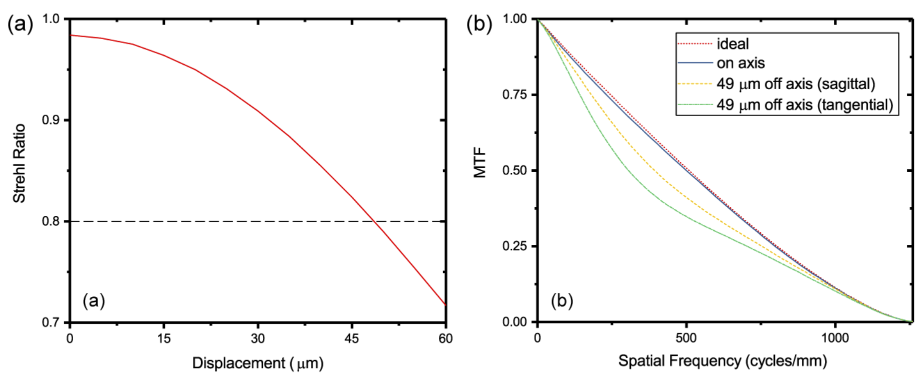

Fig. 2. (a) Simulated SR versus the displacement of point-like emitter off the optical axis. The diffraction-limited FOV is defined as the region of spot displacement where SR ≥ 0.8 (dashed line). (b) The simulated modulation transfer function (MTF) for point-like emitter on axis and 49 μm off axis. The ideal diffraction-limited MTF is also shown for comparison.

To experimentally verify the performances, one objective is built by using the standard B-coated (broad band anti-reflection coating from 650 nm to 1050 nm) singlets from Thorlabs and tested. The lens is optimized at 852 nm and the overall transmission is 93.2%. The line patterns and the 250-nm pinhole on a resolution chart (TC-RT01, Technologie Manufaktur) are imaged by using an additional $f = 1$ m projection achromatic lens (AC508-1000-B, Thorlabs). The experimental setup is displayed in Fig. 3(a), where a collimated 852-nm light source are used to illuminate the line patterns and pinholes respectively. The scattered light fields are collected by the designed objective with a 5-mm fused silica flat placed in front. The images are finally projected onto a CCD camera by the achromatic lens.

Figure 3(b) is the image of the line patterns, and the numbers mean the specification of line pairs per mm. The line pattern with 700 can be clearly resolved. The line width is 0.7 μm and the distance between the two lines is 1.4 μm. This means a resolution between 0.7 and 1.4 μm, which agree with the theoretical resolution $0.61\lambda/\mathrm{NA} = 0.96$ μm.

Optics EXPRESS

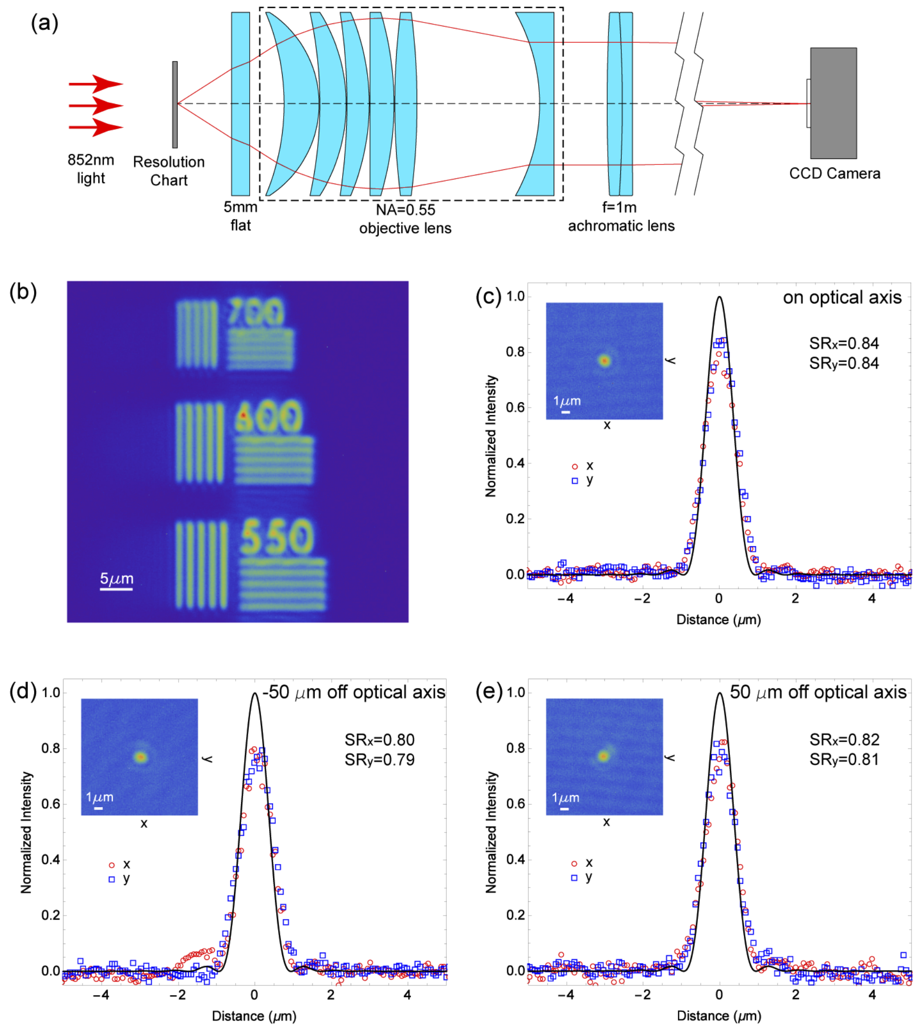

Fig. 3. (a) Scheme of experimental setup to test the performances of the NA= 0.55 objective. (b) Image of the line patterns with number 550, 600, and 700. (c)-(e) Measurement of point spread function (PSF) with the 250-nm pinhole on and ±50 μm off optical axis. The red circles and the blue squares are the normalized intensity distribution along x axis and y axis which across the intensity maxima, whereas the black curve is the ideal PSF. Insets of (c)-(e) is the image of the 250-nm pinhole on CCD camera.

To further characterize the resolving quality within the FOV, the point spread functions (PSFs) for a series of focal spots on the image plane are measured by imaging the 250-nm pinhole on the resolution chart. Because the size of the pinhole is much smaller than the wavelength, so it can be regarded as a good point-like emitter. The measured PSF for the pinhole on optical axis is shown in Fig. 3(c). The inset is the two-dimensional (2D) PSF captured by CCD camera. The solid line in main figure is the theoretical PSF. The points are the experimental data of one dimensional PSF extracted from the 2D image along the x and y axis. The experimental data is normalized to the theoretical one to have the same power. So, the maximal value in center gives the measured SR [25], which is displayed as SR_x and SR_y in the main figure with x and y being the two directions. We see the SRs on both axis are greater than 0.8, which means the

Optics EXPRESS

diffraction-limited resolution on optical axis. The PSF data on the edge of the FOV (±50 μm off the optical axis) are given by Fig. 3(d) and (e). The measured SRs are also greater than 0.8, which indicates the objective can achieve the diffraction-limited resolution within the whole FOV.

In addition to the diffraction-limit performance at 852nm and window thickness of 5 mm, the objective could also be optimized to diffraction limit at various working wavelengths and window thicknesses by only adjusting the distance between the first two lenses (LC1093 and LB1199, thickness of surface 2 in Table 1). Table 2(a) gives the optimizing results of the objective for various typical wavelengths with the window thickness fixed at 5 mm. (b) shows the example of the re-optimization for various window thickness with the wavelength fixed as 852 nm. The NA is kept as 0.55 for all of these re-optimizations.

Table 2. (a) NA= 0.55 objective reoptimized for a serial of typical wavelengths with a flat window thickness of 5 mm. (b) NA= 0.55 objective reoptimized for various window thicknesses T at the wavelength of 852 nm. The NA is kept as 0.55 for all these examples. The symbols of λ, *d*, D, and FOV indicates the working wavelength, the distance between the first two singlets, the thickness of optical flat, and the field of view, respectively.

(a)

λ (nm)	d (mm)	FOV (μm)	Transition line
852	33.92	98	Cs D2
780	33.67	87	Rb D2
671	33.17	71	Li D2
461	31.29	43	Sr
399	30.13	36	Yb

(b)

T (mm)	d (mm)	FOV (μm)
7	38.52	100
6	36.09	99
5	33.92	98
4	31.97	96
3	30.13	92

3. NA= 0.78 objective

The mechanical structure of the NA= 0.78 objective is shown in Fig. 4. Six commercial on-shelf singlets (LC1093, LB1374, LA1050, LE 1418, LE1076, and LE5802 from Thorlabs Inc.) are mounted in standard 2″ lens tube. Five are Φ2” size and one (LE5802) is Φ1” size. The Φ1” singlet is glued in a special holder and the others are mounted with standard Φ2” rings. The lens sequence follows the rule in the designing of NA= 0.55 objective. The three Meniscus lenses

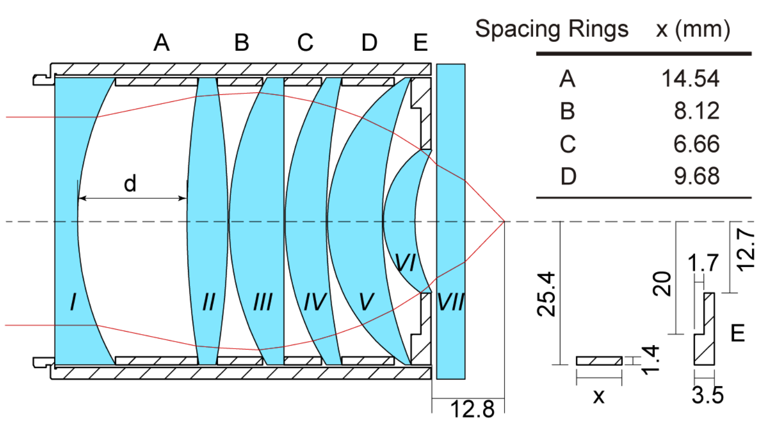

Fig. 4. Structure of the NA= 0.78 objective assembly. The singlets marked with number *I*, *II*,. . . , and *VII* are the on-shelf singlets with part number LC1093, LB1374, LA1050, LE 1418, LE1076, LE5802, and optical flat. The material of the optical flat is silica with thickness of 5 mm. The effective focal length of the objective is 23.64 mm at 852 nm.

Optics EXPRESS

have relatively shorter focal lengths, e.g., LE1418 (f = 150 mm), LE1076 (f = 100 mm), and LE5802 (f = 75 mm), and this design can increase the NA to 0.78. This objective is also initially optimized and simulated by Zemax at wavelength of 852 nm and with 5-mm silica window. The optimized objective prescription is shown in Table 3 and the Zemax file can be found in Code 1 [26].

Table 3. The prescription NA= 0.78 objective optimized at 852 nm and with 5-mm silica window (optical flat).

Surfce	Curvature (mm)	Thickness (mm)	Material	Part Number
1	∞	4	NBK7	LC1093
2	51.5	19.35 (d)	Air	
3	153.3	7.2	NBK7	LB1374
4	−153.3	0.2	Air	
5	51.5	9.7	NBK7	LA1050
6	∞	0.2	Air	
7	47.9	7.3	NBK7	LE 1418
8	119.3	0.2	Air	
9	30.3	9.7	NBK7	LE1076
10	65.8	0.2	Air	
11	15.5	5.6	CaF_2	LE5802
12	28	3.84	Air	
13	∞	5 (T)	Silica	Optical Flat
14	∞	7	Vacuum	

Figure 5 displays the simulated performance. The SR versus the focal spot displacement off the optical axis is shown in Fig. 5(a). The SR for the spot on optical axis is 0.97 with a RMS wave front error of 3%λ and the FOV is about 15 μm. The simulated MTFs for focal spots on axis and 7.5 μm off the optical axis are given by Fig. 5(b). The results imply the good imaging contrast within the whole FOV.

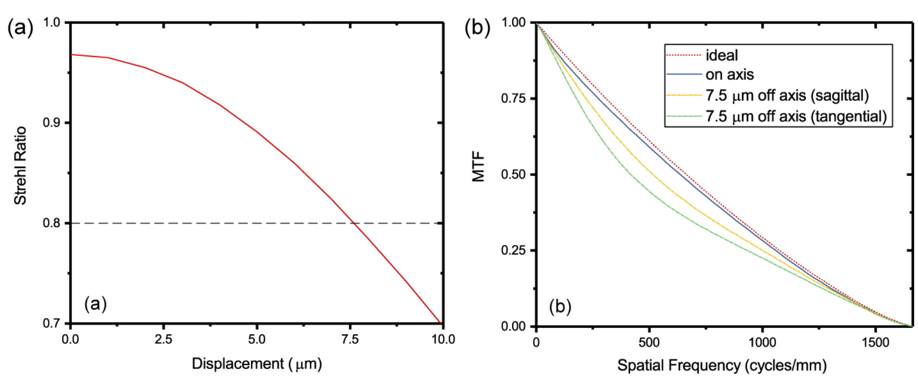

Fig. 5. (a) Simulated SR versus the displacement of point-like emitter off the optical axis. The diffraction-limited FOV is defined as the region of spot displacement where SR ≥ 0.8 (dashed line). (b) The simulated modulation transfer function (MTF) for point-like emitter on axis and 7.5 μm off axis. The ideal diffraction-limited MTF is also shown for comparison.

The objective is also built with standard B-coated singlets from Thorlabs and experimentally tested. The test setup is same to that of NA= 0.55 one [Fig. 3(a)] except the objective itself.

The overall transmission is same to the NA = 0.55 one. The image of the line patterns is shown in Fig. 6(a), and we see that the pattern with number 850 can be clearly resolved. This give a resolution between 0.6 and 1.2 μm, which is in agreement with the theoretical value $0.61\lambda/\mathrm{NA} = 0.67$ μm. The PSF and SR measured by imaging the 250-nm pinhole are displayed in Fig. 6(b)-(d). The data indicate that the objective can work with diffraction-limit within the whole FOV.

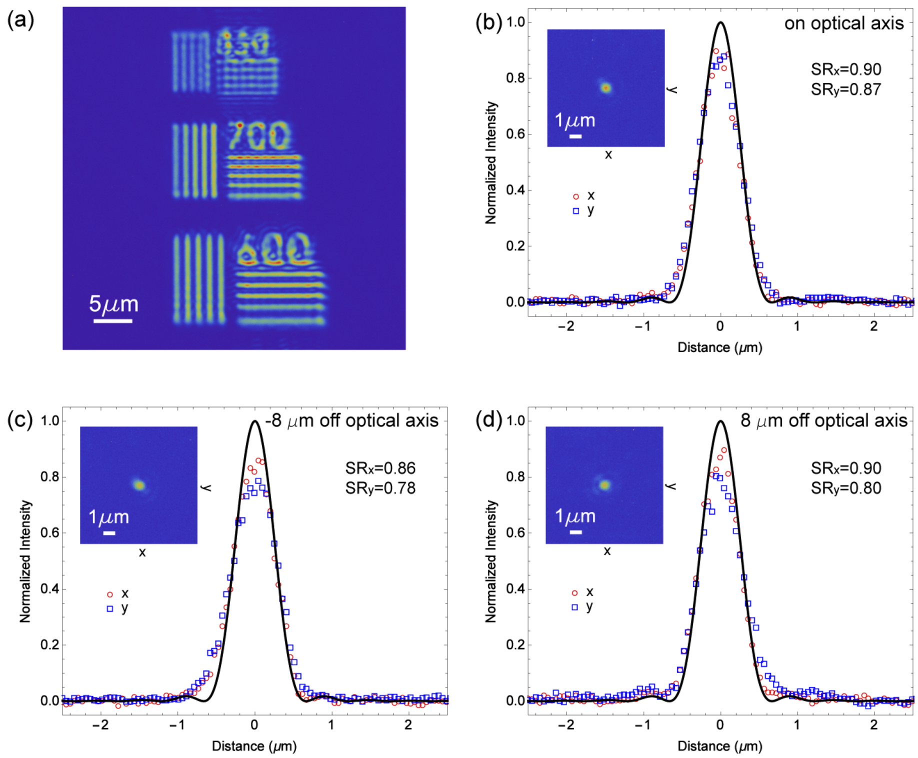

Fig. 6. (a) Image of the line patterns with number 600, 700 and 850. (b)-(d) Measurement of point spread function (PSF) with the 250-nm pinhole on and ±8 μm off optical axis. The red circles and the blue squares are the normalized intensity distribution along x axis and y axis which across the intensity maxima, whereas the black curve is the ideal PSF. Insets of (b)-(d) is the image of the 250-nm pinhole on CCD camera.

Table 4. (a) NA= 0.78 objective reoptimized for a serial of typical wavelengths with a flat window thickness of 5 mm. (b) NA= 0.78 objective reoptimized for various window thicknesses T at the wavelength of 852 nm. The NA is kept as 0.78 for all these examples. The symbols have same meaning to those in Table 2.

(a)

λ (nm)	d (mm)	FOV (μm)	Transition line
852	19.35	15	Cs D2
780	19.10	14	Rb D2
671	18.61	11	Li D2
461	16.78	7	Sr
399	15.69	6	Yb

(b)

T (mm)	d (mm)	FOV (μm)
7	30.28	7
6	24.17	12
5	19.35	15
4	15.44	16
3	12.20	12

Optics EXPRESS

Same to the NA= 0.55 one, this NA= 0.78 objective can also be reoptimized at any single wavelength from ultra-violet to near infrared and with various window thickness by only adjusting the distance between the first two lenses (LC1093 and LB1374, also the thickness of surface 2 in Table 3). Table 4(a) summarized the optimization results for a couple of typical wavelength with the window thickness fixed at 5 mm. (b) shows the examples of the reoptimizing for various window thickness at fixed wavelength of 852 nm. The NA is kept as 0.78 for all of the re-optimizations.

4. Conclusion

In this paper we present two high NA objectives ensembled entirely by commercial on-catalog singlets. The key features of two objectives optimized at 852 nm light and with a 5-mm silica window are summarized in Table 5. The performances of the two objectives are simulated by the commercial ray-tracing software and tested experimentally by imaging line patterns and 250-nm pinhole associated with a resolution chart. The measured SR indicate the diffraction-limit resolution over the full FOV.

Table 5. Key features of the two objectives with 852-nm light and 5-mm silica window.

NA	EFL (mm)	WD (mm)	FOV (μm)	Resolution (μm)
0.55	30.95	23.0	98	0.94
0.78	23.64	12.8	15	0.67

These two objectives can be reoptimized for various thickness of window at single wavelength from ultraviolet to near inferred region by only adjusting the distance between first two singlets. Thus, we believe that they are suitable for imaging and resolving individual atom of various species in either single atom arrays or optical lattices with versatile vacuum setups. Moreover, the two objectives could also be used for other applications, such as in bio-physics to monitoring the living cell or in industry to check the small structure at long working distance.

Funding

National Key Research and Development Program of China (2017YFA0304502); National Natural Science Foundation of China (11574187, 11634008, 11674203, 11974223, 11974225); Fund for Shanxi "1331 Project" Key Subjects Construction; Program for the Innovative Talents of Higher Learning Institutions of Shanxi.

Disclosures

The authors declare that there are no conflicts of interest related to this article.

References

1. J. F. Sherson, C. Weitenberg, M. Endres, M. Cheneau, I. Bloch, and S. Kuhr, “Single-atom-resolved fluorescence imaging of an atomic mott insulator,” Nature **467**(7311), 68–72 (2010).
2. C. Gross and I. Bloch, “Quantum simulations with ultracold atoms in optical lattices,” Science **357**(6355), 995–1001 (2017).
3. M. F. Parsons, F. Huber, A. Mazurenko, C. S. Chiu, W. Setiawan, K. Wooley-Brown, S. Blatt, and M. Greiner, “Site-resolved imaging of fermionic ^{6}Li in an optical lattice,” Phys. Rev. Lett. **114**(21), 213002 (2015).
4. M. Saffman, T. G. Walker, and K. Mølmer, “Quantum information with rydberg atoms,” Rev. Mod. Phys. **82**(3), 2313–2363 (2010).
5. D. S. Weiss and M. Saffman, “Quantum computing with neutral atoms,” Phys. Today **70**(7), 44–50 (2017).
6. L.-M. Duan and C. Monroe, “Colloquium: Quantum networks with trapped ions,” Rev. Mod. Phys. **82**(2), 1209–1224 (2010).
7. D. Barredo, V. Lienhard, S. de Léséleuc, T. Lahaye, and A. Browaeys, “Synthetic three-dimensional atomic structures assembled atom by atom,” Nature **561**(7721), 79–82 (2018).

Optics EXPRESS

8. A. Kumar, T.-Y. Wu, F. Giraldo, and D. S. Weiss, "Sorting ultracold atoms in a three-dimensional optical lattice in a realization of maxwell's demon," Nature **561**(7721), 83–87 (2018).
9. D. Barredo, S. de Léséleuc, V. Lienhard, T. Lahaye, and A. Browaeys, "An atom-by-atom assembler of defect-free arbitrary two-dimensional atomic arrays," Science **354**(6315), 1021–1023 (2016).
10. M. Endres, H. Bernien, A. Keesling, H. Levine, E. R. Anschuetz, A. Krajenbrink, C. Senko, V. Vuletic, M. Greiner, and M. D. Lukin, "Atom-by-atom assembly of defect-free one-dimensional cold atom arrays," Science **354**(6315), 1024–1027 (2016).
11. H. Labuhn, D. Barredo, S. Ravets, S. de Léséleuc, T. Macrì, T. Lahaye, and A. Browaeys, "Tunable two-dimensional arrays of single rydberg atoms for realizing quantum ising models," Nature **534**(7609), 667–670 (2016).
12. J. Zhang, G. Pagano, P. W. Hess, A. Kyprianidis, P. Becker, H. Kaplan, A. V. Gorshkov, Z.-X. Gong, and C. Monroe, "Observation of a many-body dynamical phase transition with a 53-qubit quantum simulator," Nature **551**(7682), 601–604 (2017).
13. W. Alt, "An objective lens for efficient fluorescence detection of single atoms," Optik **113**(3), 142–144 (2002).
14. X. Li, F. Zhou, M. Ke, P. Xu, X.-D. He, J. Wang, and M.-S. Zhan, "High-resolution ex vacuo objective for cold atom experiments," Appl. Opt. **57**(26), 7584–7590 (2018).
15. J. D. Pritchard, J. A. Isaacs, and M. Saffman, "Long working distance objective lenses for single atom trapping and imaging," Rev. Sci. Instrum. **87**(7), 073107 (2016).
16. L. M. Bennie, P. T. Starkey, M. Jasperse, C. J. Billington, R. P. Anderson, and L. D. Turner, "A versatile high resolution objective for imaging quantum gases," Opt. Express **21**(7), 9011–9016 (2013).
17. S. Li, G. Li, W. Wu, Q. Fan, Y. Tian, P. Yang, P. Zhang, and T. Zhang, "High-numerical-aperture and long-working-distance objective for single-atom experiments," Rev. Sci. Instrum. **91**(4), 043104 (2020).
18. I. H. A. Knottnerus, S. Pyatchenkov, O. Onishchenko, A. Urech, F. Schreck, and G. A. Siviloglou, "Microscope objective for imaging atomic strontium with 0.63 micrometer resolution," Opt. Express **28**(8), 11106–11116 (2020).
19. E. Haller, J. Hudson, A. Kelly, D. Cotta, B. Peaudecerf, G. Bruce, and S. Kuhr, "Single-atom imaging of fermions in a quantum-gas microscope," Nat. Phys. **11**(9), 738–742 (2015).
20. R. Yamamoto, J. Kobayashi, T. Kuno, K. Kato, and Y. Takahashi, "An ytterbium quantum gas microscope with narrow-line laser cooling," New J. Phys. **18**(2), 023016 (2016).
21. S. M. Mansfield and G. S. Kino, "Solid immersion microscope," Appl. Phys. Lett. **57**(24), 2615–2616 (1990).
22. C. Robens, S. Brakhane, W. Alt, F. Kleißler, D. Meschede, G. Moon, G. Ramola, and A. Alberti, "High numerical aperture (na = 0.92) objective lens for imaging and addressing of cold atoms," Opt. Lett. **42**(6), 1043–1046 (2017).
23. M. W. Gempel, T. Hartmann, T. A. Schulze, K. K. Voges, A. Zenesini, and S. Ospelkaus, "An adaptable two-lens high-resolution objective for single-site resolved imaging of atoms in optical lattices," Rev. Sci. Instrum. **90**(5), 053201 (2019).
24. Li Shaokang, Li Gang, Yang Pengfei, Wang Zhihui, Zhang Pengfei, and Zhang Tiancai, "Zemax file for NA = 0.55 objective," figshare, 2020, https://doi.org/10.6084/m9.figshare.13134935.
25. H. Gross, H. Zügge, M. Peschka, and F. Blechinger, *Handbook of Optical Systems, Aberration Theory and Correction of Optical Systems* (Wiley-VCH, 2015).
26. Li Shaokang, Li Gang, Yang Pengfei, Wang Zhihui, Zhang Pengfei, and Zhang Tiancai, "Zemax file for NA = 0.78 objective," figshare, 2020, https://doi.org/10.6084/m9.figshare.13134950.